Formation and dissociation reactions of complexes involving interstitial carbon and oxygen defects in silicon

H. M. Ayedh* and E. V. Monakhov
University of Oslo, Department of Physics/Center for Materials Science and Nanotechnology, P.O. Box 1048 Blindern, N-0316 Oslo, Norway

J. Coutinho
I3N, Department of Physics, University of Aveiro, Campus Santiago, 3810-193 Aveiro, Portugal

(Received 5 March 2020; accepted 14 May 2020; published 1 June 2020)

We present a detailed first-principles study which explores the configurational space along the relevant reactions and migration paths involving the formation and dissociation of interstitial carbon-oxygen complexes, C_iO_i and C_iO_{2i}, in silicon. The formation/dissociation mechanisms of C_iO_i and C_iO_{2i} are found as occurring via capture/emission of mobile C_i impurities by/from O complexes anchored to the lattice. The lowest activation energies for dissociation of C_iO_i and C_iO_{2i} into smaller moieties are 2.3 and 3.1 eV, respectively. The first is compatible with the observed annealing temperature of C_iO_i, which occurs at around 400 °C, and below the threshold for O_i diffusion. The latter exceeds significantly the measured activation energy for the annealing of C_iO_{2i} ($E_a = 2.55$ eV). We propose that instead of dissociation, the actual annealing mechanism involves the capture of interstitial oxygen by C_iO_{2i}, thus being governed by the migration barrier of O_i ($E_m = 2.53$ eV). The study is also accompanied by measurements of hole capture cross sections and capture barriers of C_iO_i and C_iO_{2i}. In combination with previously reported data, we find thermodynamic donor transitions which are directly comparable to the first-principles results. The two levels exhibit close features, conforming to a model where the electronic character of C_iO_{2i} can be described by that of C_iO_i perturbed by a nearby O atom.

DOI: 10.1103/PhysRevMaterials.4.064601

I. INTRODUCTION

Understanding the evolution of point defect complexes in silicon (Si) during device processing is highly significant to the industry of electronics and photovoltaics. Carbon and oxygen are the most common foreign species in monocrystalline Si wafers grown by the Czochralski technique (Cz-Si), with concentrations of about 10^{16} cm^{-3} and over 10^{17} cm^{-3}, respectively. They are predominantly present in the as-grown Si material in the form of substitutional carbon (C_s) or interstitial oxygen (O_i) impurities.

Despite being electrically inert, C_s and O_i can have significant influence on the electrical properties of Si wafers/samples. A conspicuous example is the formation of the so-called thermal double donors, which comprise a family of oxygen aggregates that lead to a considerable increase in free-electron concentration. The effect occurs upon heat treatments of O-rich Si in the temperature range of 400–500 °C, while it is strongly suppressed in samples where in addition to oxygen, carbon is also present in a high concentration [1,2]. Another prominent example is the so-called light-induced degradation (LID) of n^+p-Si solar cells where the p-type layer is boron (B) doped [3,4]. Recent measurements and theory indicate that the defect comprises a complex made of one boron atom and an oxygen dimer [5].

Both C_s and O_i can trap intrinsic defects, resulting in electrically active complexes that can travel long distances in the Si [6]. Interstitial oxygen comprises a twofold coordinated O atom sitting near the center of Si-Si bonds. Migration of O_i proceeds via consecutive jumps between nearest bonds with an activation energy $E_m = 2.53$ eV [7]. It is primarily a trap for vacancy-type defects, in particular the monovacancy (V), thus leading to formation of the vacancy-oxygen complex which has an acceptor level at $E_c - 0.17$ eV [8,9].

On the other hand, C_s is an efficient trap for self-interstitials (Si_i), where Si_i partially takes the place of the C atom, which is displaced from the substitutional site to become interstitial carbon (C_i). This reaction has been termed as *kick-out mechanism* [10]. C_i shows a split-interstitial configuration, comprising a C-Si dimer sharing a lattice site and aligned along ⟨001⟩ [11–13]. C_i produces both acceptor ($E_c - 0.10$ eV) and donor ($E_v + 0.28$ eV) levels [14] (E_c and E_v denote the conduction and valence band edge energies, respectively). The defect becomes mobile just above room temperature (RT), and depending on doping type, anneals out with an activation energy of ∼0.7–0.87 eV (assigned to its migration barrier), yielding a diffusivity in the range 10–15 cm^2/s [11,15,16].

In carbon-rich Si, mobile C_i defects are most likely to be captured by C_s, forming interstitial-carbon–substitutional-carbon complexes (C_iC_s) [17]. In oxygen-rich Si, the dominant trap for the mobile C_i is O_i [18], leading to formation of interstitial-carbon–interstitial-oxygen complexes (C_iO_i). C_iO_i has a deep donor level at $E_v + 0.36$ eV, and that has been corroborated by both electron paramagnetic resonance (EPR)

*hussein.ayedh@smn.uio.no

and deep-level transient spectroscopy (DLTS) measurements [19,20]. We should add that substitutional boron (B_s) is known to compete with C_s for the capture of Si_i defects by a similar kick-out mechanism, suppressing the generation of C_i, and therefore, the formation of C_iO_i [21,22]. When B_s is the dominant trap, the resulting boron interstitial (B_i) defects become mobile at RT and ultimately form B_iO_i and B_iB_s complexes, depending on the relative content of B_s and O_i in the samples [21–24].

C_iO_i has been extensively investigated by several spectroscopic techniques. The defect gives rise to a conspicuous zero-phonon emission line at 789 meV, the so-called C-line in the photoluminescence (PL) spectra, at low temperatures ($T \leqslant 20$ K) [25–27]. This energy is close to the gap width (E_g) subtracted by the hole binding energy of the donor level ($E_{\text{C-line}} \approx E_g - 0.36$ eV), and was interpreted as resulting from the recombination energy of a diffuse electron possessing a conduction-band-like character with a hole tightly bound (∼0.36 eV binding energy) to neutral C_iO_i. From Fourier-transform infrared (FTIR) absorption spectroscopy, two main local vibrational mode (LVM) bands associated with C_iO_i are also well established. At low temperatures, they appear at 865 cm^{-1} [known as C(3) band] and at 1116 cm^{-1} [26,28–30]. From *ab initio* local density functional calculations, Jones and Öberg [31], and more recently Coutinho *et al.* [29], showed that in the C_iO_i ground state, both O and C are threefold coordinated. This configuration was shown to be necessary in order to account for the electrical, optical, and magnetic resonance experiments [19,26,28–30].

More recently, Khirunenko *et al.* [32,33] found that the formation of C_iO_i is more complex than previously thought, and reported the formation of metastable configurations of C_iO_i during isochronal annealing of irradiated Si in the temperature range 280–360 K. These findings were interpreted as the formation of a precursor (labeled $C_iO_i^*$) before reaching the ground state [32–34]. The proposed geometry for the metastable defect consisted of C_i and O_i defects lying on a common {110} plane and separated by a Si-Si bond, essentially retaining their threefold and twofold coordination of their individual structures, respectively. From annealing data, the $C_iO_i^* \rightarrow C_iO_i$ conversion was estimated to be activated by a barrier of ∼1 eV [34]. Although capture/transformation/dissociation mechanisms have not been explored by theory, the binding energy of $C_iO_i^*$ was calculated to be ∼0.7 eV, about 1 eV lower than that estimated for C_iO_i (ground state) [33].

The evolution of C_iO_i upon post-irradiation thermal treatments has been studied for decades, but surprisingly, few studies addressed the kinetics and annealing mechanisms of C_iO_i. The defect is generally considered to be stable up to 400 °C [22,27,28]. By monitoring the C(3) absorption band in high-fluence MeV electron-irradiated Cz samples [28], first order annealing kinetics was inferred with activation energy and pre-exponential factor of 2.0 eV and 3×10^{12} s^{-1}, respectively. On the basis of these results, C_iO_i was tentatively suggested to anneal out via dissociation ($C_iO_i \rightarrow C_i + O_i$).

From PL measurements, the loss of the C-line during heat treatments at 350–450 °C has been observed to be accompanied by the formation of the so-called P-line at 767 meV [27,35,36]. Several photoluminescence studies have argued that the P-line is associated with carbon- and oxygen-related defects, most likely involving an oxygen dimer bonded to C_i [27,35–38]. The PL spectra of the C- and P-lines exhibit almost identical properties as well as very similar effective-masslike excited states. Furthermore, like the C center, the point group symmetry of the P center is also C_{1h}.

Assuming that like the C-line, the P-line results from recombination of an effective-masslike electron with a hole on a deep donor state, from the difference of their zero-phonon energies we may infer that the P center gives rise to a donor transition 22 meV above that of C_iO_i, i.e., at about $E_v + 0.38$ eV. In fact, a correlation has been recently found between the P-line and a DLTS peak at $E_v + 0.39$ eV that forms upon the annealing of C_iO_i [39,40]. This peak was tentatively assigned to an interstitial-carbon–interstitial-dioxygen complex (C_iO_{2i}). The annealing of C_iO_i was proposed to occur via dissociation into C_i and O_i, with the released C_i defects being subsequently trapped by O_{2i} [39]. Considering that the above suggests that trapping of C_i by progressively larger oxygen aggregates tends to raise a donor level towards higher energies within the band gap, it is important to determine the mechanisms involved in the operating reactions, and ultimately the impact of the reaction products in terms of recombination power.

Recently, Ayedh *et al.* [41] studied the annealing kinetics of C_iO_{2i} in irradiated *p*-type (B-doped) Cz-Si samples by monitoring the $E_v + 0.39$ eV hole trap via DLTS. The trap anneals out according to first order kinetics, exhibiting an activation energy of ∼2.55 eV, and a pre-exponential factor in the range $(2–30) \times 10^{12}$ s^{-1}. From the kinetics and deduced prefactor (of the order of the Debye frequency of Si), it was suggested that the annealing of C_iO_{2i} occurs via dissociation, rather than being a diffusion-limited process. To clarify this and other issues related to the formation and dissociation of carbon-oxygen complexes, we performed a detailed theoretical study which explores the configurational space along relevant reaction and migration paths involving C and O species in Si. The study is also accompanied by measurements of capture cross sections and barriers for the capture of holes by C_iO_i and C_iO_{2i}, allowing us to accurately locate their thermodynamic donor transitions.

II. METHOD DETAILS

A. Calculation details

First-principles calculations were performed using the Vienna *ab initio* simulation package (VASP) [42–45], employing the projector-augmented wave (PAW) method for the treatment of the core electrons [46]. A basis set of plane waves with kinetic energy of up to 400 eV was used to describe the Kohn-Sham states. All many-body energies reported were evaluated self-consistently, using the hybrid density functional of Heyd-Scuseria-Ernzerhof (HSE06) [47,48], up to a numerical accuracy of 10^{-7} eV. Hybrid density functionals perform relatively better in terms of the calculated band structure, when compared with semilocal functionals, including those using the generalized gradient approximation (GGA) [49]. The GGA was however employed for the search of ground-state and saddle-point structures along the minimum

energy paths (MEP) of atomistic mechanisms. All structures were optimized until forces on atoms were below 0.01 eV/Å. The two-step method—first involving a calculation of a GGA-level structure followed by a single-point energy calculation within HSE06, was shown to lead to numerical error bars below 10 meV for relative energies, including formation energies and migration barriers [50,51]. These tests also apply to the methods used below to find saddle point energies, which are simply a sequence of structural relaxations subject to a particular set of constraints.

We used 216-atom supercells of silicon (with cubic shape), obtained by replication of $3 \times 3 \times 3$ conventional cells, in which carbon and oxygen atoms were inserted to produce CO-related defects. The defects considered were all interstitials, namely carbon (C_i), oxygen (O_i), oxygen dimer (O_{2i}), carbon-oxygen (C_iO_i), and carbon-dioxygen (C_iO_{2i}). The equilibrium (calculated) lattice parameters of Si was $a = 5.4318$ Å, matching the experimental value of $a = 5.4310$ Å. The Brillouin zone (BZ) of GGA- and HSE06-level calculations was sampled at Γcentered $2 \times 2 \times 2$ (Γ-2^3) and $1 \times 1 \times 1$ (Γ-point) **k**-point meshes, respectively.

To investigate defect migration and transformation processes, we employed a combination of *nudged elastic band* (NEB) [52,53] and *dimer* [54] methods (at the GGA level). For the NEB calculations, initial and final (frozen) geometries were at the limits of a sequence of 9–11 intermediate images, which were created at first hand by linear interpolation and adjusted to avoid unphysical bond lengths. Saddle-point search calculations involved a first step consisting of a fast exploratory NEB run with the Brillouin zone being sampled at the Γ point. On a subsequent step, we increased the **k**-point sampling density to Γ-2^3, and refined the exploratory MEP by either employing the climbing-image NEB method [55] or by performing a dimer search. The dimer run was initiated using the two higher-energy structures obtained from the previous exploratory NEB step. Finally, the resulting highest-energy configuration along each MEP (the saddle point) was taken in order to calculate its total energy within HSE06.

B. Measurement details

A set of n^+p diodes were prepared (fabrication details are described in Ref. [41]) on a *p*-type (boron doped) Cz-Si wafer with resistivity of ∼14 Ω cm, corresponding to a net carrier concentration of about $\sim 1 \times 10^{15}$ cm^{-3} at RT, as determined by capacitance-voltage (C-V) measurements with a 1 MHz probe frequency. The oxygen and carbon concentration in the wafers was 7×10^{17} and $\leqslant 2 \times 10^{16}$ cm^{-3}, respectively, as determined by secondary ion mass spectrometry (SIMS). Aluminum (Al) Ohmic contacts were deposited by electron beam evaporation on the front side (n^+ layer) and silver paste was applied on the back side of the samples to form an Ohmic contact. The fabricated n^+p diodes were subjected to annealing at 300 °C for 26 h in N_2 atmosphere and then were irradiated with 1.8 MeV protons at RT to doses of 1×10^{13} cm^{-2}. After irradiation, the samples were annealed at 400 °C for 1.5 h in order to anneal out all the radiation-produced point defects, except C_iO_i which exhibited a dominating DLTS peak. One of the samples was subjected to a multiple-step annealing at 400 °C for about 30 h in total in order to achieve a complete annealing of the C_iO_i complex and formation of C_iO_{2i} (see Ref. [41] for further details). C-V and DLTS measurements were employed after each annealing step for characterizing the samples using a refined version of the setup described in Ref. [56], equipped with a closed-cycle He cryostat.

In DLTS, the reverse bias quiescent voltage was kept at −10 V, the filling pulse was 50 ms long at 0 V bias, and the sample temperature was scanned between 50 and 300 K. The DLTS signal was extracted from the recorded capacitance transients applying a lock-in and a high resolution weighting function, so-called GS4 [57], with six different rate windows in the range of (20–640 ms)$^{-1}$. The C_iO_i and C_iO_{2i} defects were monitored via their respective deep levels at $E_v + 0.36$ eV and $E_v + 0.39$ eV. These correspond to DLTS peak positions at 173 and 190 K, respectively, when employing a rate window of 640 m s^{-1} and the GS4 weighting functions. Hole capture cross sections (σ) were measured for C_iO_i and C_iO_{2i} traps by varying the filling pulse duration from 10 ns to 10 μs and recording the amplitude of the level signal. During these measurements a single rate window was used for each capture cross section measurement and the sample temperature was kept constant within $T = T_{max} \pm 0.1$ K, where T_{max} is the temperature that corresponds to maximum DLTS signal for a specific rate window.

III. RESULTS

A. Migration energies of elementary defects

We start by reporting on some properties of basic elements that participate in the reactions addressed in Sec. III B, namely O_i, O_{2i}, C_i, C_iO_i, and C_iO_{2i}.

In agreement with previously experimental and theoretical studies [11–13,58], we find that the ground-state structure of interstitial carbon (C_i) in Si comprises a C-Si split interstitial, possessing dangling bonds on both C and Si atoms. As shown in Figs. 1(a) and 1(b), the C-Si dimer is aligned along the ⟨001⟩ direction, and both atoms share a lattice site.

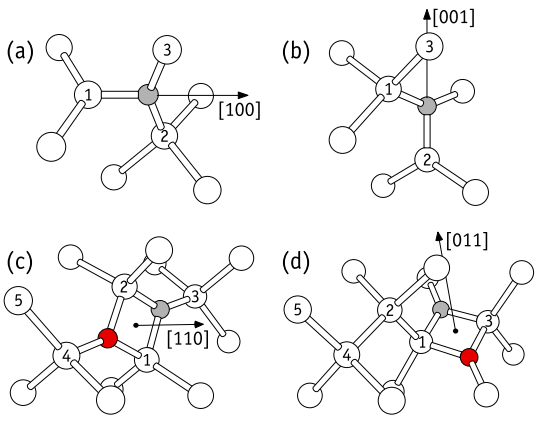

FIG. 1. Initial (a) and (c) and final (b) and (d) structures for single jumps during the migration of C_i and C_iO_i defects in silicon. Some ligands are labeled with numbers in order to assist the reader in the identification of the Si neighbors before and after the jumps. Oxygen, carbon, and silicon atoms are represented in red, gray, and white, respectively. Some crystallographic directions are also represented to indicate the alignment of the defects with respect to the host lattice.

As for interstitial oxygen (O_i) in Si, the resulting ground state structure is also in line with the widely accepted model, according to which the O atom sits near the bond center site, forming a *puckered* Si-O-Si unit [59–61]. The orbiting motion of the O atom around the ⟨111⟩ axis of the perfect Si-Si bond, as well as its motion across the bond center site, involve surmounting rather shallow energy barriers of the order of 10 meV.

The minimum-energy structure of the oxygen dimer is the so-called *staggered* configuration [60–62], where two O atoms occupy neighboring bond center sites, thus connecting to a common Si atom. In this geometry, the O atoms in the Si-O-Si-O-Si structure are displaced in a staggered way. This minimizes the departure from the sp^3 bond angles involving the central Si atom and its O neighbors [60–62].

For the C_iO_i and C_iO_{2i} complexes, we found that in both cases the defect core comprises a squarelike structure involving C, O, and two Si atoms. Figures 1(c) and 1(d) represent two orientations of C_iO_i in Si. For the case of C_iO_{2i}, the structure is similar to that of C_iO_i, although an additional O atom is connected to Si atoms number 4 and 5 in Fig. 1(c). Hence, the complex is essentially a staggered O_{2i} next to C_i.

We also found a metastable $C_iO_i^*$ complex, identical to that reported by Khirunennko *et al.* [33], consisting of C_i and twofold coordinated O_i impurities separated by a Si-Si bond and sharing the same plane. The $C_iO_i^*$ complex was found 1.0 eV above the ground state, i.e., with a binding energy of 0.56 eV with respect to isolated C_i and O_i impurities.

In the analysis of the defect reactions described in Sec. III B, we assume that the migration barriers for C_i, O_i, and O_{2i} are, respectively, (0.73 ± 0.05), (2.53 ± 0.03), and (2.02 ± 0.01) eV as derived from experiments [63–65]. The migration mechanisms of all three defects are well established theoretically [61,66]. Hence, a calculation of the respective barriers would provide us with an idea of the error bar of the methodology. As mentioned in Sec. II A, the search for saddle points was conducted along the configurational space between initial and final ground states structures.

The MEP for migration of C_i was found to involve a change in the defect alignment within the Si lattice. Initial and final configurations are illustrated in Figs. 1(a) and 1(b). Accordingly, the C atom performs an *out-of-plane* jump, leading to a change of orientation of the main ⟨100⟩ symmetry axis. This mechanism was earlier found by Capaz *et al.* [66], and according to our calculations corresponds to a MEP with a total barrier of $E_m = 0.76$ eV. This figure matches recent annealing experiments carried out in n^+p diodes under reverse bias [63], where a barrier for the migration of carbon interstitial in the neutral charge state was measured as $E_m = 0.73$ eV. The energy barrier for the *in-plane* jump of C_i is about 1.6 eV high, essentially due to the fact that the carbon atom has to travel through a high-energy twofold coordinated Si-C-Si structure.

Interstitial oxygen migrates by hopping between neighboring (puckered) bond center sites. The saddle-point configuration is commonly referred to as Y-lid [61], and it is analogous to the stable configuration of C_i depicted in Fig. 1 (the C atom being replaced by O). Our calculations indicate that the Y-lid structure of O_i is 2.63 eV above the ground state, overestimating the experimental figure by a mere 0.1 eV. This result is in line with the 2.7 eV barrier height reported previously using hybrid density functional calculations [67]. As for the oxygen dimer, the saddle point for migration is attained when both O atoms display threefold coordination (see Fig. 7 in Ref. [61]). Here we found that the relevant structure along the path is 1.87 eV above the ground state, about 0.1 eV below the measured value [65]. These results suggest that the error bar regarding the energy barriers to be discussed below is about 0.1 eV. This is approximately twice the error in the measured barrier of C_i and about 10 times the error in the measured barriers of O_i and O_{2i} [63–65].

Like the carbon interstitial, the MEP for migration C_iO_i also involves a change in the defect alignment within the Si lattice. Initial and final configurations are shown in Figs. 1(c) and 1(d). C and O atoms in C_iO_i jump off the {110} symmetry plane, in a sequential manner—first the carbon atom, then the oxygen. The second step has the highest barrier, leading to an overall migration barrier of $E_m = 2.45$ eV. This is 0.65 eV lower than the barrier for in-plane migration, and such a large figure derives from the nearly independent jump of the O atom.

Below we will argue that migration of C_iO_i is actually an unlikely event due to the fact that dissociation is governed by a lower barrier.

B. Formation and dissociation of C_iO_i and C_iO_{2i}

Before proceeding, we leave a few words about notation. Let us consider that A and B stand for either O_i, C_i, or a complex made of any (including more than one) of these species. Infinitely separated defects A and B are represented as A + B (e.g., $C_iO_i + O_i$); Complexes involving close pairs of A and B atoms separated by two or more Si atoms, but still sharing the same supercell volume, are represented as A-B (e.g., C_iO_i-O_i); complexes involving A and B moieties connected to a common Si atom are termed AB (e.g., C_iO_{2i}). We did not find stable complexes involving direct C-O or O-O bonds. Di-carbon complexes were not investigated.

Regarding the designation of the saddle-point structure along a particular MEP, we found it useful to highlight the atoms that move most during the respective mechanism. This is done by enclosing the moving species within parentheses. For the dissociation of C_iO_{2i}, for instance, if the jumping moiety is the carbon atom (leaving O_{2i} behind), the carbon species is enclosed within parentheses. Hence, a first step for the dissociation reaction is cast as

$$C_iO_{2i} \xrightarrow{(C_i)O_{2i}} C_i\text{-}O_{2i}, \tag{1}$$

which involves a detachment of the carbon atom from O_{2i}, followed by a second step

$$C_i\text{-}O_{2i} \xrightarrow{(C_i)+O_{2i}} C_i + O_{2i}, \tag{2}$$

describing the migration of C_i away from O_{2i}.

Figure 2 shows a reaction energy diagram accounting for the interactions between one C and two O atoms in silicon. Each state involves three interstitial atoms, being represented by a horizontal segment in the energy scale, a state label, and its relative energy, in eV, enclosed within square brackets. Starred energies were obtained with help of experimentally obtained migration barriers of C_i, O_i, and O_{2i}. All energies are

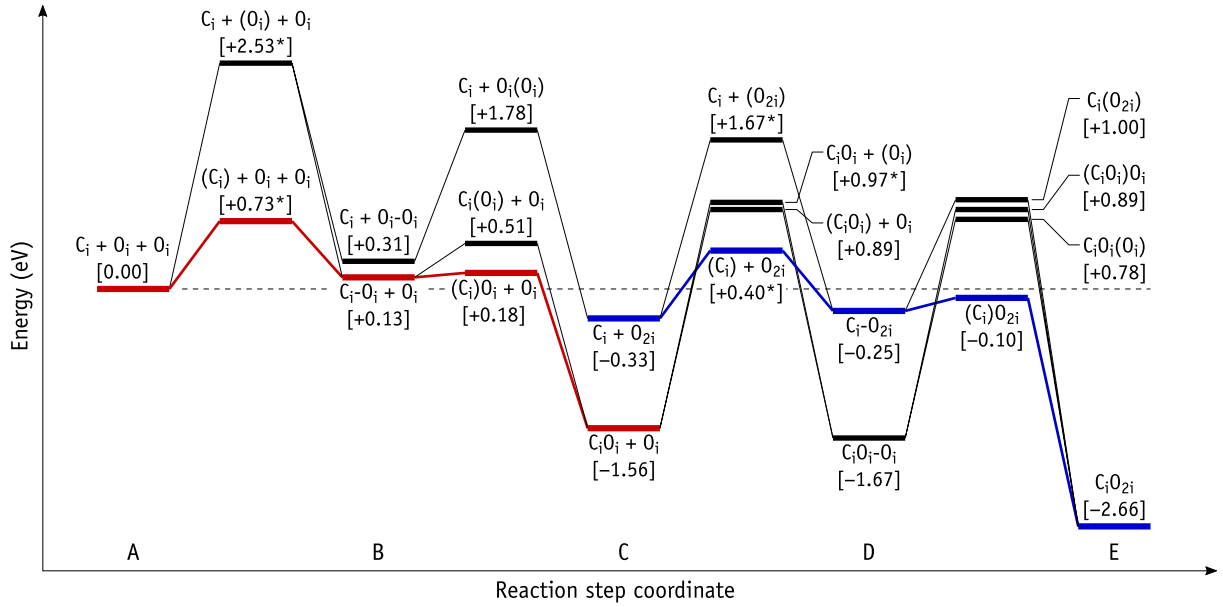

FIG. 2. Reaction energy diagram involving interstitial carbon (C_i) and two interstitial oxygen impurities (O_i) in silicon. The diagram highlights in red and blue the most favorable reactions paths describing the formation/dissociation of C_iO_i and C_iO_{2i} complexes, respectively. Reactions proceed through sequential transformations between reaction steps denoted with letters A–E. These correspond to stable states represented by a thick horizontal segment, a state label, and its relative energy within square brackets. See text for details regarding label notation. Intermediate states (between stable steps) are saddle points and correspond to the summit of the minimum energy path that separates neighboring stable states. Atoms or groups of atoms that jump during each step are represented within parentheses. The origin of the energy coordinate is shown as a dashed horizontal line. All energies are in eV.

relative to the $C_i + O_i + O_i$ state in step A. This is indicated by the wide horizontal dashed line, and stands for uncorrelated C_i and two O_i impurities. Each step (A–E) groups one or more stable (ground or metastable) states. Different states within each step are not necessarily close in configurational space. States between neighboring steps are saddle points. The purpose of the thin lines connecting the horizontal state segments is to relate every pair of stable states with at least one saddle point. They also provide guidance to the reader in the identification of mechanisms along the reactions steps. The atoms that move most during a transition are enclosed within parentheses (see above).

Figure 2 also highlights the most favorable reactions paths for the formation/dissociation of C_iO_i (A ↔ C) and C_iO_{2i} (C ↔ E) complexes in red and blue, respectively. Formation and dissociation processes read from left to right and vice versa, respectively. The ground states in steps C and E correspond to the C_iO_i and C_iO_{2i} complexes, respectively. From their relative energies we find that the binding energies of C_i to O_i and to O_{2i} are $E_b = 1.56$ and 2.33 eV as obtained from the energy balance of

$$C_i + O_i + O_i\ (A) \rightarrow C_iO_i + O_i\ (C) + [E_b = 1.56\ \text{eV}] \quad (3)$$

and

$$C_i + O_{2i}\ (C) \rightarrow C_iO_{2i}\ (E) + [E_b = 2.33\ \text{eV}], \quad (4)$$

respectively, where reaction steps are indicated within parentheses. The magnitude of the binding energies indicate a strong thermodynamic drive for formation of these complexes. The binding energy of C_iO_i is also in line with previous calculations, where E_b values were found in the range 1.6–1.7 eV [29,33,68]. The binding energy between two interstitial O atoms is found from the energy difference of states in steps A and C, namely

$$C_i + O_i + O_i\ (A) \rightarrow C_i + O_{2i}\ (C) + E_b, \quad (5)$$

with $E_b = 0.33$ eV, nicely matching the 0.3 eV found experimentally by Murin *et al.* [69].

Migration barriers of C_i (0.73 eV), O_i (2.53 eV), O_{2i} (2.02 eV), and C_iO_i (2.45 eV) were considered for the saddle-point transitions A → B and C → D. The reactants are at least two independent defects, one of which is a diffusing species (indicated within parentheses). The products involve metastable precursors (steps B and D) that can be converted into stable defects in steps C and E, respectively. The mechanisms and saddle points for these conversions, namely B → C and D → E, are indicated between the respective reaction steps. Again, the moving atoms are enclosed within parentheses.

The minimum energy path for formation of C_iO_i is clearly limited by the migration barrier of C_i and not by a capture barrier. This is compatible with the observation of C_iO_i in irradiated material at room temperature. Accordingly, the saddle-point energy for

$$C_i\text{-}O_i + O_i\ (B) \xrightarrow{(C_i)O_i+O_i} C_iO_i + O_i\ (C) \quad (6)$$

is located at 0.18 eV in the energy scale, below the 0.76 eV of the state involving the migration of C_i. Obviously the large migration barrier of O_i inhibits the formation of C_iO_i via migration of oxygen.

Note that the left reactant in reaction (6) is distinct from the metastable $C_iO_i^*$ precursor reported in Ref. [33]. In the C_i-O_i structure, both C and O atoms are separated by a Si-Si bond, but unlike $C_iO_i^*$, they do not share the same crystallographic plane. According to the energy scale of Fig. 2, $C_iO_i^*$ is located at -0.56 eV. Direct conversion of $C_iO_i^*$ into C_iO_i via an in-plane jump of carbon or oxygen atoms involves surmounting a barrier of at least 2.0 eV. Alternatively, the transformation of $C_iO_i^*$ first into triclinic C_i-O_i (step B) followed by conversion into C_iO_i (step C) has an overall barrier of only 0.94 eV. This is in excellent agreement with the measurements of Abdullin *et al.* [34], who reported a 1 eV activation energy for the growth of C_iO_i DLTS signal at the expense of another peak related to its precursor.

Dissociation of C_iO_i essentially consists of the reversed formation mechanism (red line in Fig. 2). The overall activation energy for dissociation, $E_d = 2.29$ eV, is also governed by the migration of C_i, which follows from its off-plane detachment from oxygen in a first stage [reversal of reaction (6)]. This result slightly overestimates the $\sim$2 eV from early measurements of the activation energy for the annealing of C_iO_i [28,70].

The alternative mechanism, where instead of C_i motion, the first stage involves a detachment of O_i from C_iO_i,

$$C_iO_i + O_i\ (C) \overset{C_i(O_i)+O_i}{\longrightarrow} C_i\text{-}O_i + O_i\ (B) \tag{7}$$

was also inspected. Reaction (7) starts from ground state at step C (red) and has a barrier of 2.07 eV with saddle point at $+0.51$ eV shown in Fig. 2 in black. However, since C_i still has to escape from oxygen, the overall barrier for dissociation is also $E_d = 2.29$ eV. This dissociation route is nevertheless unlikely to occur due to a higher first stage barrier.

Now we turn to C_iO_{2i}. Its formation can occur either (i) via further accumulation of oxygen in C_iO_i, which means starting with reactants $C_iO_i + O_i$ (step C, red line) in Fig. 2, or (ii) from reaction between C_i and O_{2i}, where the starting conditions are represented by $C_i + O_{2i}$ (step C, blue line). Of course, in Cz-Si, where the concentration of oxygen is much larger than that of carbon, the initial state of option (ii) can only be achieved upon release of C_i defects from the overwhelming concentration of oxygen traps. Hence, option (ii) actually involves two simultaneous reactions, namely (ii.1) the dissociation of C_iO_i (reaction C $\rightarrow$ A) and (ii.2) capture of C_i by O_{2i} to the more stable C_iO_{2i} complex (reaction C $\rightarrow$ E). The alternative formation mechanism implying the capture of a diffusing O_{2i} by C_i is not physically probable due to the high barrier involved.

According to Fig. 2, the formation mechanism (i) can occur via migration of O_i with an overall barrier of 2.53 eV, or via migration of C_iO_i with an activation energy of 2.45 eV. However, these reaction routes are shortcut by dissociation of C_iO_i (which has an energy barrier of 2.29 eV only), thus providing the necessary conditions for activation of the formation mechanism (ii). Like C_iO_i, the formation of C_iO_{2i} via mechanism (ii) along the blue line of Fig. 2 is only limited by the migration barrier of C_i. However, because the first stage reaction (ii.1) actually involves the dissociation of C_iO_i (reaction C $\rightarrow$ A), the formation mechanism of C_iO_{2i} is effectively activated by the dissociation barrier of C_iO_i, i.e., $E_a = 2.29$ eV. Note that the state $(C_i) + O_i + O_i$ at 0.73 eV which limits the dissociation of C_iO_i to make carbon interstitials available, is higher in energy than $(C_i) + O_{2i}$ at 0.40 eV governing the capture of C_i by O_{2i}. This picture explains the observed correlation between the dissociation of C_iO_i and formation of C_iO_{2i} [39–41].

Regarding the dissociation of C_iO_{2i}, we calculated four possible scenarios which differ in the initial E $\rightarrow$ D step as depicted in Fig. 2, and can be summarized as follows: (i) jump of C_i away from C_iO_{2i}, leaving O_{2i} behind; (2) detachment of O_i from C_iO_{2i} leaving a C_iO_i complex; (3) jump of O_{2i} away from C_iO_{2i}, leaving a C_i defect, and (4) detachment of a C_iO_i complex from C_iO_{2i}, thus leaving O_i. Figure 2 clearly indicates that mechanism (i) is the most favorable dissociation route, showing an activation energy of $E_d = 3.06$ eV. This figure is about 0.5 eV higher than what was recently observed by some of us during annealing experiments [41]. We can only reconcile the calculations with the measurements if we assume that, instead of a dissociation, the relevant annealing mechanism involves the capture of interstitial oxygen by C_iO_{2i}, namely

$$C_iO_{2i} + O_i \overset{C_iO_{2i}+(O_i)}{\longrightarrow} C_iO_{3i}, \tag{8}$$

thus explaining the measured activation energy $E_a = 2.55$ eV for the annealing of C_iO_{2i} [41], which is virtually identical to the migration barrier of O_i. We found that the formation of C_iO_{3i} according to reaction (8) is energetically favorable and corresponds to a lowering of the energy by $E_b = 0.76$ eV. Here the ground state structure of C_iO_{3i} consisted of a staggered oxygen trimer next to C_i. The binding energy of C_i to O_{3i} was calculated as $E_b = 2.56$ eV. This figure follows the trend shown by $E_b = 2.33$ and 1.56 eV as obtained for the analogous quantity regarding the attachment of C_i to O_{2i} and O_i, respectively [see reactions (3) and (4)]. The proposed mechanism as described by reaction (8) is also compliant with the observed first order kinetics of the annealing—the huge concentration of O_i is effectively invariant during the process.

In Ref. [41], an attempt rate for the annealing kinetics of C_iO_{2i} was measured as $\nu_\infty = (2\text{–}30) \times 10^{12}$ s^{-1}. This figure is in line with the Debye frequency of Si, suggesting that the annealing should be prompted by atomic vibrations. However, our proposal, according to which C_iO_{2i} anneals out due to capture of mobile O_i impurities, is challenged by the fact that ν_∞ is two orders of magnitude slower than the analogous figure obtained for O_i diffusivity in silicon [7]. The latter is obviously too high to be described as a simple phonon-assisted jump and, as far as we know, there is no clear explanation for such an anomaly. At the moment we can only infer that the forward rate of reaction (8) is limited by a phonon-assisted process, and therefore governed by a physics that somehow differs from that of the migration of isolated O_i. Hence, while the activation energy for the annealing of C_iO_{2i} corresponds to the large migration barrier of oxygen at remote locations from C_iO_{2i}, the measured attempt frequency in the 10^{13}-Hz range may simply reflect the kinetics of the slower final steps, when both impurities are in close proximity, which cannot be described as isolated O_i jumps anymore, but rather as a restructuring of a C_iO_{3i} complex.

We end this section with a few considerations on the charge state dependence of formation and dissociation of C_iO_i and

C_iO_{2i} complexes. First, the above results refer to neutral defects and essentially they are valid for intrinsic material or doped-Si subject to annealing ($T \sim 300$–$500\,^\circ$C).

Second, we note that the formation and dissociation mechanisms do not involve long range Coulomb interactions between reactants. Hence, in *p*-type or *n*-type Si, the energies of the stable states in steps A, C, and E should be lowered by an amount that corresponds to the depth of the hole or electron traps of C_i, C_iO_i, or C_iO_{2i}. Analogously, saddle-point energies should consider a charge state effect. In this case, both "red" and "blue" MEPs of Fig. 2 are limited by the migration barrier of C_i. Therefore, if the thermodynamic conditions are such that the Fermi level is above $E_c - 0.12$ eV [58] or below $E_v + 0.28$ eV [12], the C_i defect is negatively or positively charged, so that migration barriers for C_i^- or C_i^+ should be considered, respectively. For instance, in heavily doped *p*-type Si, the migration barrier of C_i^+ was measured as $E_m = 0.89$ eV. Considering the hole trap energies of C_i ($E_v + 0.28$ eV) and C_iO_i ($E_v + 0.36$ eV), we estimate activation energies for formation and dissociation of C_iO_i of $E_a = 0.89$ eV and $E_a = 2.53$ eV, respectively. These figures are slightly larger than the analogous quantities reported above for neutral defects (0.73 and 2.29 eV, respectively).

C. Electronic properties

In a recent study, {C,O}-rich Si samples were irradiation at room temperature and annealed at 400 °C for 30 h in order to anneal out C_iO_i and form the C_iO_{2i} [41]. The evolution of the defects was monitored by DLTS via observation of the corresponding hole traps with activation energy for hole emission of $\Delta E_h = 0.36$ eV and $\Delta E_h = 0.39$ eV. In order to obtain the thermodynamic transition levels, a capture barrier has to be subtracted from ΔE_h values, and after that we can compare the observed transitions with corresponding calculations based on ground state energies. Below we present results from measurements of the capture barriers of C_iO_i and C_iO_{2i}, which supplement the study of Ref. [41].

The hole capture cross section (σ) of C_iO_i and C_iO_{2i} was measured at different temperatures and compared for both complexes. Values of σ as a function of the inverse of the absolute temperature are plotted in Fig. 3. The σ values were extracted from the observed amplitude of the DLTS peak as a function of the filling pulse duration (between 10 ns and 10 μs) at sample temperatures in the range 170–215 K. For very short pulses (10–300 ns), the number of filled C_iO_i and C_iO_{2i} traps was negligible. On the other hand, for pulses longer than 3 μs both signals saturated due to complete filling of the traps. The two levels exhibit close capture cross sections ($\sim 9 \times 10^{-17}$ cm^2 for C_iO_i versus $\sim 8 \times 10^{-17}$ cm^2 for C_iO_{2i}) with very weak impact of the temperature variation. However, σ is a temperature-dependent quantity which can be described as

$$\sigma = \sigma_\infty \exp(-\Delta E_\sigma / k_B T), \tag{9}$$

where σ_∞ is the direct capture cross section (high temperature limit), ΔE_σ is the thermally activated hole capture barrier, and k_B is the Boltzmann constant. Values of ΔE_σ and σ_∞ for C_iO_i and C_iO_{2i} were extracted by fitting Eq. (9) to the measured data as depicted in Fig. 3. We found that ΔE_σ is very small

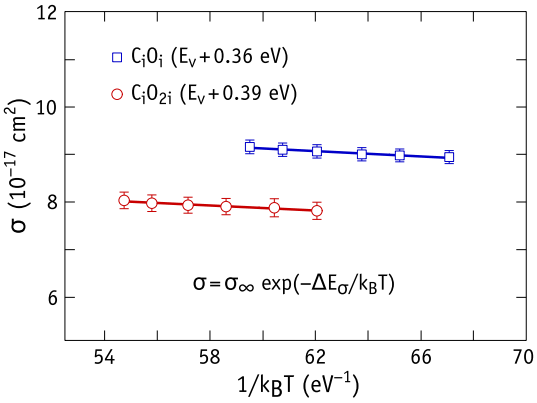

FIG. 3. Temperature dependence of the hole capture cross section (σ) of C_iO_i and C_iO_{2i} traps. $\sigma(T)$ for hole capture by neutral C_iO_i and C_iO_{2i} shows very week temperature dependency due to the very small capture barrier for both complexes (as extracted from the slopes of linear fittings). E_v, σ_∞, and ΔE_σ stand for the valence band top energy, the direct hole capture cross section, and respective thermally activated capture barrier. Straight lines are linear fits of $\sigma(T)$ to the data.

and almost identical for both defects, ~3 meV for C_iO_i and ~4 meV for C_iO_{2i}. This result is in line with the model where the C_iO_{2i} hole trap can be described as a C_iO_i trap perturbed by the presence of a nearby interstitial oxygen atom.

Activation energies of hole emission and apparent capture cross sections for C_iO_i and C_iO_{2i} as reported in Ref. [41] are listed in Table I. These data are also accompanied by direct capture cross sections and capture barriers for both complexes as obtained from the present measurements. In addition, the measured and calculated (see below) electronic levels [$E(0/+) - E_v$] of C_iO_i and C_iO_{2i} are also included.

The capture barriers for C_iO_i and C_iO_{2i} are very small, and therefore, the measured activation energies for hole emission essentially represent the location of the donor transition with respect to the valence band top. Furthermore, no variation was found for the hole emission rate of both C_iO_i and C_iO_{2i} traps with the application of different electric fields during the DLTS experiments. The lack of a Poole-Frenkel effect indicates that both levels are likely to correspond to donor transitions.

A transition level between two charge states, say q and q', of a defect (with q being more negative than q') is defined as

$$E(q/q') = -\frac{E^{(q)}(R) - E^{(q')}(R')}{q - q'}, \tag{10}$$

TABLE I. Activation energies for hole emission (ΔE_h) and apparent capture cross sections (σ_a) (from Ref. [41]), direct capture cross sections (σ_∞) and capture barriers (ΔE_σ) (this work) of C_iO_i and C_iO_{2i} complexes in Si. Capture cross sections and energies are given in cm^2 and eV, respectively. Measured and calculated donor levels, $E(0/+) - E_v$, are also reported.

	Hole trap data				$E(0/+) - E_v$	
	ΔE_h	σ_a	σ_∞	ΔE_σ	Measured	Calculated
C_iO_i	0.36	1×10^{-15}	1.1×10^{-16}	0.003	0.36	0.30
C_iO_{2i}	0.39	2×10^{-15}	9.6×10^{-17}	0.004	0.39	0.33

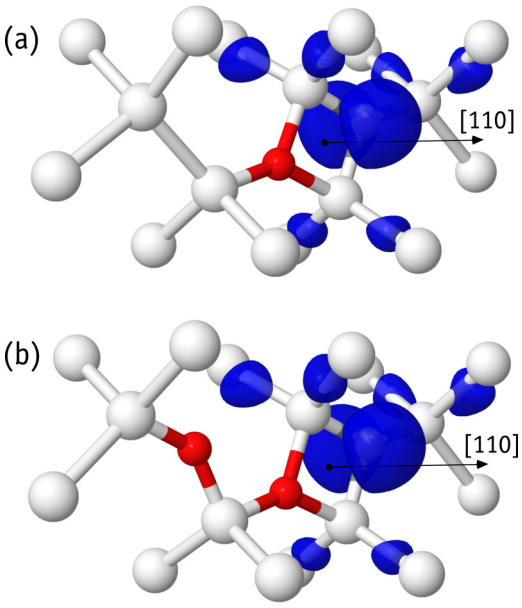

FIG. 4. Isosurface of the electron density related to the highest occupied state (donor state) of (a) C_iO_i and (b) C_iO_{2i}. The isosurface cut-off value is identical for both cases, $\rho_{cut} = 0.001$ Bohr^{-3}. The viewpoint is analogous to that of Fig. 1(c). The [110] crystallographic direction is perpendicular to the mirror plane of the defects.

where $E^{(q)}$ is the energy of the supercell with the defect in charge state q and R a generalized coordinate representative of the defect configuration. Equation (10) accounts for the fact that charge states q and q' may correspond to radically different atomistic geometries R and R', respectively (which is not the present case). The use of periodic boundary conditions imply that the supercell is always neutral irrespectively of the number of electrons in the system. To mitigate this spurious effect, energies in Eq. (10) are offset by a periodic charge correction according to Freysoldt *et al.* [71].

In order to cast the levels in a way that they can be compared to the experiments, i.e., $E(0/+) - E_v$, we have to calculate the energy of the valence band top. This is done by using Eq. (10) for the case of a bulk (defect-free) supercell, $E_v = E_{bulk}(0/+)$.

The calculated donor levels of C_iO_i and C_iO_{2i} are shown in the rightmost column of Table I. They are underestimated with respect to the observations by 60 meV, but significantly they account for the observed relative depth, i.e., the donor transition of C_iO_{2i} is 30 meV above the donor transition of C_iO_i.

The hole traps arise from a fully occupied p-like state centered on the carbon atom, and lying deep in the band gap. Figure 4 depicts the donor state (Kohn-Sham state) within the gap in the form of an electron density isosurface (blue), related to the highest occupied state of neutral C_iO_i and C_iO_{2i} defects. The carbon atom is hidden by the large p-orbital-like shape near the arrow that indicates the [110] direction. There is no apparent difference between the two defects. This is consistent with the nearly identical characteristics determined for both, namely the activation energy for hole emission, the capture barriers, and capture cross sections.

The fact that the donor level of C_iO_{2i} is slightly higher (30 meV) in the gap, can be explained by the repulsion of the donor electrons on the p state by the additional and highly electronegative O atom. This effect is analogous to that invoked to explain the rise of the donor transitions of the thermal double donors in Si and Ge, where the increasing number of oxygen atoms accumulated on each donor leads to progressively shallower levels [72].

IV. CONCLUSIONS

We presented a detailed model regarding the formation and dissociation mechanisms of carbon-oxygen complexes, involving interstitial carbon and interstitial oxygen impurities. The results are based on hybrid density functional theory. We also supplement previous experimental data with capture kinetics measurements, which allowed us to estimate and compare the capture barriers of C_iO_i and C_iO_{2i}.

Like C_iO_i, the C_iO_{2i} complex is made of a squarelike core structure involving C, O, and two Si atoms. Both defects show large binding energies,

$$C_i + O_i + O_i \xrightarrow{E_m=0.73\ \text{eV}} C_iO_i + O_i + [E_b = 1.56\ \text{eV}], \quad (11)$$

$$C_i + O_{2i} \xrightarrow{E_m=0.73\ \text{eV}} C_iO_{2i} + [E_b = 2.33\ \text{eV}], \quad (12)$$

which are suggestive of a high thermal stability. The kinetics of both reactions above are thermally activated by the migration barrier of C_i ($E_m = 0.73$ eV). However, in O-rich material and below the annealing temperature of C_iO_i ($\sim$400 °C), reaction (11) will dominate due to the large concentration O_i traps for the fast-diffusing C_i (in comparison to the concentration of O_{2i}).

Dissociation of C_iO_i is simply governed by reaction (11) in the backwards direction. Now the carbon detaches and escapes from O_i. The calculated overall barrier is $E_d = 1.56 + 0.73 = 2.29$ eV. This result implies that C_iO_i should dissociate at a slightly lower temperature than that for migration of O_i (with an activation barrier of about 2.5 eV).

As referred above, around room temperature, C_i defects become mobile and are quickly consumed by abundant O_i to form C_iO_i. The C_iO_{2i} is observed only after (1) annealing out C_iO_i by reversing reaction (11), and (2) the released C_i impurities travel and find O_{2i}, according to reaction (12), ending up in a more stable complex ($E_b = 2.33$ eV). This process is limited by step 1 (annealing of C_iO_i), meaning that it is thermally activated by the dissociation barrier of C_iO_i ($E_d = 2.29$ eV). Again, this happens at temperatures below the threshold for migration of O_i.

The annealing of C_iO_{2i} was found to follow from the capture of mobile O_i impurities by C_iO_{2i} as

$$C_iO_{2i} + O_i \xrightarrow{E_m=2.53\ \text{eV}} C_iO_{3i}, \quad (13)$$

whose kinetics is limited by the migration barrier of interstitial oxygen impurities ($E_m = 2.53$ eV). This picture accounts well for the annealing measurements of C_iO_{2i}, which was found to be thermally activated by a barrier $E_a = 2.55$ eV. Dissociation of C_iO_{2i} into smaller moieties had barriers invariably above 3 eV.

The electronic properties of C_iO_i and C_iO_{2i} were compared by calculating their donor levels, as well as measuring their respective capture cross sections. Both theory and experiments converge well—C_iO_i has a donor transition at $E_c + 0.36$ eV, only 30 meV below the analogous transition of C_iO_{2i}.

ACKNOWLEDGMENTS

Financial support by the Norwegian Research Council through the research project OxSil (No. 254977) is gratefully acknowledged. The Research Council of Norway is also acknowledged for the support to the Norwegian Micro- and Nano-Fabrication Facility, NorFab (Project No. 245963). H.M.A. thanks the Faculty of Mathematics and Natural Sciences/University of Oslo, Norway for the Kristine Bonnevie travel grant to support his research visit to University of Aveiro. J.C. thanks the support of the i3N project, References No. UIDB/50025/2020 and No. UIDP/50025/2020, financed by the Fundação para a Ciência e a Tecnologia in Portugal.

[1] W. Kaiser, H. L. Frisch, and H. Reiss, Phys. Rev. **112**, 1546 (1958).
[2] A. R. Bean and R. C. Newman, J. Phys. Chem. Solids **33**, 255 (1972).
[3] J. Schmidt, Solid State Phenomena **95–96**, 187 (2003).
[4] J. Schmidt and K. Bothe, Phys. Rev. B **69**, 024107 (2004).
[5] M. Vaqueiro-Contreras, V. P. Markevich, J. Coutinho, P. Santos, I. F. Crowe, M. P. Halsall, I. Hawkins, S. B. Lastovskii, L. I. Murin, and A. R. Peaker, J. Appl. Phys. **125**, 185704 (2019).
[6] S.-R. G. Christopoulos, D. C. Parfitt, E. N. Sgourou, C. A. Londos, R. V. Vovk, and A. Chroneos, J. Mater. Sci.: Mater. Electron. **27**, 11268 (2016).
[7] R. C. Newman, J. Phys.: Condens. Matter **12**, R335 (2000).
[8] G. D. Watkins and J. W. Corbett, Phys. Rev. **121**, 1001 (1961).
[9] Y.-H. Lee and J. W. Corbett, Phys. Rev. B **13**, 2653 (1976).
[10] G. D. Watkins, *Radiation Damage in Semiconductors* (Dunod, Paris, 1965).
[11] G. D. Watkins and K. L. Brower, Phys. Rev. Lett. **36**, 1329 (1976).
[12] Y. H. Lee, L. J. Cheng, J. D. Gerson, P. M. Mooney, and J. W. Corbett, Solid State Commun. **21**, 109 (1977).
[13] P. Leary, R. Jones, S. Öberg, and V. J. B. Torres, Phys. Rev. B **55**, 2188 (1997).
[14] C. A. Londos, Phys. Rev. B **35**, 6295 (1987).
[15] A. K. Tipping and R. C. Newman, Semicond. Sci. Technol. **2**, 315 (1987).
[16] J. Tersoff, Phys. Rev. Lett. **64**, 1757 (1990).
[17] K. P. O'Donnell, K. M. Lee, and G. D. Watkins, Physica B+C **116**, 258 (1983).
[18] C. A. Londos, Phys. Rev. B **37**, 4175 (1988).
[19] J. M. Trombetta and G. D. Watkins, Appl. Phys. Lett. **51**, 1103 (1987).
[20] M. T. Asom, J. L. Benton, R. Sauer, and L. C. Kimerling, Appl. Phys. Lett. **51**, 256 (1987).
[21] P. M. Mooney, L. J. Cheng, M. Süli, J. D. Gerson, and J. W. Corbett, Phys. Rev. B **15**, 3836 (1977).
[22] L. C. Kimerling, M. T. Asom, J. L. Benton, P. J. Drevinsky, and C. E. Caefer, Mater. Sci. Forum **38–41**, 141 (1989).
[23] G. D. Watkins, Phys. Rev. B **12**, 5824 (1975).
[24] L. Vines, E. V. Monakhov, A. Y. Kuznetsov, R. Kozłowski, P. Kaminski, and B. G. Svensson, Phys. Rev. B **78**, 085205 (2008).
[25] K. Thonke, G. D. Watkins, and R. Sauer, Solid State Commun. **51**, 127 (1984).
[26] G. Davies, A. S. Oates, R. C. Newman, R. Woolley, E. C. Lightowlers, M. J. Binns, and J. G. Wilkes, J. Phys. C: Solid State Phys. **19**, 841 (1986).
[27] W. Kürner, R. Sauer, A. Dörnen, and K. Thonke, Phys. Rev. B **39**, 13327 (1989).
[28] B. G. Svensson and J. L. Lindström, Phys. Status Solidi (a) **95**, 537 (1986).
[29] J. Coutinho, R. Jones, P. R. Briddon, S. Öberg, L. I. Murin, V. P. Markevich, and J. L. Lindström, Phys. Rev. B **65**, 014109 (2001).
[30] L. I. Murin, V. P. Markevich, J. L. Lindström, M. Kleverman, J. Hermansson, T. Hallberg, and B. G. Svensson, Solid State Phenom. **82-84**, 57 (2001).
[31] R. Jones and S. Öberg, Phys. Rev. Lett. **68**, 86 (1992).
[32] L. I. Khirunenko, Y. V. Pomozov, N. A. Tripachko, M. G. Sosnin, A. V. Duvanskii, L. I. Murin, J. L. Lindström, S. B. Lastovskii, L. F. Makarenko, V. P. Markevich, and A. R. Peaker, Solid State Phenom. **108–109**, 261 (2005).
[33] L. I. Khirunenko, M. G. Sosnin, Y. V. Pomozov, L. I. Murin, V. P. Markevich, A. R. Peaker, L. M. Almeida, J. Coutinho, and V. J. B. Torres, Phys. Rev. B **78**, 155203 (2008).
[34] K. A. Abdullin, B. N. Mukashev, M. F. Tamendarov, and T. B. Tashenov, Phys. Lett. A **144**, 198 (1990).
[35] G. Davies and R. C. Newman, Carbon in monocrystalline silicon, in *Handbook on Semiconductors*, edited by S. Mahajan (Elsevier, Amsterdam, 1994), Vol. 3, p. 1557.
[36] G. Davies, S. Hayama, L. Murin, R. Krause-Rehberg, V. Bondarenko, A. Sengupta, C. Davia, and A. Karpenko, Phys. Rev. B **73**, 165202 (2006).
[37] N. Fukuoka, K. Atobe, and M. Honda, Jpn. J. Appl. Phys. **29**, 1625 (1990).
[38] O. O. Awadelkarim, A. Henry, B. Monemar, J. L. Lindström, Y. Zhang, and J. W. Corbett, Phys. Rev. B **42**, 5635 (1990).
[39] N. Ganagona, B. Raeissi, L. Vines, E. V. Monakhov, and B. G. Svensson, Phys. Status Solidi (c) **9**, 2009 (2012).
[40] B. Raeissi, N. Ganagona, A. Galeckas, E. V. Monakhov, and B. G. Svensson, Solid State Phenom. **205–206**, 224 (2013).
[41] H. M. Ayedh, A. A. Grigorev, A. Galeckas, B. G. Svensson, and E. V. Monakhov, Phys. Status Solidi A **216**, 1800986 (2019).
[42] G. Kresse and J. Hafner, Phys. Rev. B **47**, 558 (1993).
[43] G. Kresse and J. Hafner, Phys. Rev. B **49**, 14251 (1994).
[44] G. Kresse and J. Furthmüller, Phys. Rev. B **54**, 11169 (1996).
[45] G. Kresse and J. Furthmüller, Comput. Mater. Sci. **6**, 15 (1996).
[46] P. E. Blöchl, Phys. Rev. B **50**, 17953 (1994).
[47] J. Heyd, G. E. Scuseria, and M. Ernzerhof, J. Chem. Phys. **118**, 8207 (2003).
[48] A. V. Krukau, O. A. Vydrov, A. F. Izmaylov, and G. E. Scuseria, J. Chem. Phys. **125**, 224106 (2006).

[49] J. P. Perdew, K. Burke, and M. Ernzerhof, Phys. Rev. Lett. **77**, 3865 (1996).
[50] J. D. Gouveia and J. Coutinho, Electron. Struct. **1**, 015008 (2019).
[51] M. E. Bathen, J. Coutinho, H. M. Ayedh, J. Ul Hassan, I. Farkas, S. Öberg, Y. K. Frodason, B. G. Svensson, and L. Vines, Phys. Rev. B **100**, 014103 (2019).
[52] G. Mills and H. Jónsson, Phys. Rev. Lett. **72**, 1124 (1994).
[53] G. Mills, H. Jónsson, and G. K. Schenter, Surf. Sci. **324**, 305 (1995).
[54] G. Henkelman and H. Jónsson, J. Chem. Phys. **111**, 7010 (1999).
[55] G. Henkelman, B. P. Uberuaga, and H. Jónsson, J. Chem. Phys. **113**, 9901 (2000).
[56] B. G. Svensson, K.-H. Rydén, and B. M. S. Lewerentz, J. Appl. Phys. **66**, 1699 (1989).
[57] A. A. Istratov, J. Appl. Phys. **82**, 2965 (1997).
[58] L. W. Song and G. D. Watkins, Phys. Rev. B **42**, 5759 (1990).
[59] D. R. Bosomworth, W. Hayes, A. R. L. Spray, and G. D. Watkins, Proc. R. Soc. London Ser. A **317**, 133 (1970).
[60] M. Pesola, J. von Boehm, T. Mattila, and R. M. Nieminen, Phys. Rev. B **60**, 11449 (1999).
[61] J. Coutinho, R. Jones, P. R. Briddon, and S. Öberg, Phys. Rev. B **62**, 10824 (2000).
[62] M. Needels, J. D. Joannopoulos, Y. Bar-Yam, and S. T. Pantelides, Phys. Rev. B **43**, 4208 (1991).
[63] S. B. Lastovskii, V. E. Gusakov, V. P. Markevich, A. R. Peaker, H. S. Yakushevich, F. P. Korshunov, and L. I. Murin, Phys. Status Solidi (a) **214**, 1700262 (2017).
[64] J. W. Corbett, R. S. McDonald, and G. D. Watkins, J. Phys. Chem. Solids **25**, 873 (1964).
[65] V. Quemener, B. Raeissi, F. Herklotz, L. I. Murin, E. V. Monakhov, and B. G. Svensson, J. Appl. Phys. **118**, 135703 (2015).
[66] R. B. Capaz, A. Dal Pino, and J. D. Joannopoulos, Phys. Rev. B **50**, 7439 (1994).
[67] J. F. Binder and A. Pasquarello, Phys. Rev. B **89**, 245306 (2014).
[68] D. Backlund and S. Estreicher, Phys. B: Condens. Matter **401–402**, 163 (2007).
[69] L. I. Murin, T. Hallberg, V. P. Markevich, and J. L. Lindström, Phys. Rev. Lett. **80**, 93 (1998).
[70] B. G. Svensson and J. L. Lindström, Phys. Rev. B **34**, 8709 (1986).
[71] C. Freysoldt, J. Neugebauer, and C. G. Van de Walle, Phys. Rev. Lett. **102**, 016402 (2009).
[72] J. Coutinho, R. Jones, L. I. Murin, V. P. Markevich, J. L. Lindström, S. Öberg, and P. R. Briddon, Phys. Rev. Lett. **87**, 235501 (2001).